HHS Public Access

Author manuscript

J Bone Miner Res. Author manuscript; available in PMC 2018 November 18.

Published in final edited form as:

J Bone Miner Res. 2018 April ; 33(4): 691–703. doi:10.1002/jbmr.3342.

Monocyte-specific knockout of C/ebpα results in osteopetrosis phenotype, blocks bone loss in ovariectomized mice and reveals an important function of C/ebpα in osteoclast differentiation and function.

Wei Chen, MD[1,*], **Guochun Zhu**[1], **Joel Jules, PhD**[1], **Diep Nguyen**[1], and **Yi-Ping Li, PhD**[1,*]

[1]Department of Pathology, University of Alabama, Birmingham, AL 35294.

Abstract

CCAAT/enhancer-binding protein α (C/ebpα) is critical for osteoclastogenesis by regulating osteoclast (OC) lineage commitment and is also important for OC differentiation and function *in vitro*. However, the role of C/ebpα in postnatal skeletal development has not been reported owing to lethality in *C/ebpα*$^{-/-}$ mice from hypoglycemia within 8 hours after birth. Herein, we generated conditional knockout mice by deleting the *C/ebpα* gene in monocyte via LysM-Cre to examine its role in OC differentiation and function. C/ebpα$^{f/f}$LysM-Cre mice exhibited postnatal osteopetrosis due to impaired osteoclastogenesis, OC lineage priming defects, as well as defective OC differentiation and activity. Furthermore, our *ex-vivo* analysis demonstrated that *C/ebpα* conditional deletion significantly reduced OC differentiation, maturation, and activity while mildly repressing macrophage development. At the molecular level, C/ebpα deficiency significantly suppresses the expressions of OC genes associated with early stages of osteoclastogenesis as well as genes associated with OC differentiation and activity. We also identified numerous C/ebpα critical cis-regulatory elements on the Cathepsin K promoter which allow C/ebpα to significantly upregulate Cathepsin K expression during OC differentiation and activity. In pathologically induced mouse model of osteoporosis, C/ebpα deficiency can protect mice against ovariectomy-induced bone loss, uncovering a central role for C/ebpα in osteolytic diseases. Collectively, our findings have further established C/ebpα as a promising therapeutic target for bone loss by concurrently targeting OC lineage priming, differentiation and activity.

Keywords

genetic animal models; transcriptional factors; osteoclast; osteopetrosis; osteoporosis

[*]Address Correspondence to: **Yi-Ping Li, PhD,** Department of Pathology, University of Alabama, SHEL 810, 1825 University Blvd., Birmingham, AL 35294, Tel: (205) 975-2606, Fax: (205) 975-4919, yipingli@uabmc.edu. **Wei Chen, MD,** Department of Pathology, University of Alabama, SHEL 815, 1825 University Blvd., Birmingham, AL 35294, Tel: (205) 975-2605, Fax: (205) 975-4919, weichen@uabmc.edu.

Authors' roles: Study design: YPL, WC. Study conduct: WC, GZ and YPL. Data collection and analysis: WC, GZ, DN and YPL. Drafting manuscript: YPL, WC, GZ, JJ and DN. Revising manuscript: YPL, WC, GZ, JJ and DN. All authors approved the final version of the manuscript for submission. YPL (yipingli@uabmc.edu) and WC (weichen@uabmc.edu) take responsibility for the integrity of data analysis

Disclosures: The authors declare no conflicts of interest.

Additional supporting information has been included with the submission.

Introduction

Osteoclasts (OCs) are multinucleated giant cells that are critical for bone development and homeostasis. OCs originate from monocytic precursors of the hematopoietic cell lineage upon stimulation with the macrophage-colony stimulation factor (M-CSF) and receptor activator of nuclear factor-κβ (RANK) ligand (RANKL) (1). M-CSF maintains the proliferation and survival of OC precursors, and RANKL is required for OC differentiation, survival, and activity. During the early stages of osteoclastogenesis, RANKL strongly upregulates several key transcription factors, such as Finkel-Biskis-Jinkins osteosarcoma oncogene (c-Fos), proviral integration 1 (Pu.1), and nuclear factor of activated T-cells, C1 to induce OC lineage commitment which is preceded the cell differentiation (1,2). Nfatc1 is a master regulator of OC differentiation through its indispensable role in inducing various maker genes, such as tartrate resistant acid phosphatase 5 (TRAP), matrix metallopeptidase 9 (Mmp 9), cathepsin K (Ctsk), and V-proton pump, H+ transporting (vacuolar proton pump) member I (Atp6i), which are critical for terminal OC differentiation and activity (1).

Excessive bone resorption from enhanced OC formation and activity are mainly responsible for the bone loss associated with many bone diseases, including osteoporosis, rheumatoid arthritis, and periodontal diseases (3). Normal osteoclastic bone resorption involves the removal of the mineral components of bone through extracellular acidification orchestrated by many genes including Atp6i and Mmp9, which is followed by degradation of the organic constituent of bone by proteases such as *Ctsk*. We previously identified Atp6i as a putative OC-specific proton pump subunit and showed that Atp6i deletion results in a severe osteopetrosis in mice due to impaired extracellular acidification (4,5). Similarly, Ctsk is induced by RANKL during OC differentiation and activity and is highly expressed in OC (6,7). Also, mice deficient in the *Ctsk* gene are osteopetrotic from defective OC activity.

CCAAT/enhancer binding protein α (*C/ebpa*) is a transcription factor of the C/EBP family of transcription factors that carry out critical functions in hematopoiesis and granulopoiesis through its ability to bind on gene promoters to regulate gene expression (8). C/ebpα can dimerize via its leucine zipper domain at the C terminal to bind DNA and promote gene expression through its N-terminal trans-activation domain (9,10). Global deletion of the *C/ebpa* gene in mice leads to death within 8 hours of birth from hypoglycemia stemming from hepatic glycogenesis and impaired myeloid cell differentiation (10). Notably, we have recently demonstrated that C/ebpα is not only critical for OC lineage commitment, but is also important for OC differentiation and activity. Consistently, newborn $C/ebpa^{-/-}$ mice displayed osteopetrosis from impaired OC development. However, the roles of C/ebpα in postnatal skeletal OC formation and activity have not been demonstrated due to the early lethality of $C/ebpa^{-/-}$ mice.

Given that OC develops from monocyte precursors, and *C/ebpa* is critical for lineage fate decision during early hematopoietic development (11–17), we generated a *C/ebpa* monocyte-specific conditional knockout model using the LysM-Cre cell line to examine its role in OC differentiation during postnatal skeletal development. We demonstrated that the monocyte-specific conditional ablation of *C/ebpa* in mice resulted in osteopetrosis from impaired OC lineage priming, differentiation, and function. Furthermore, we showed that C/

ebpα functions by regulating the earlier known OC transcription factors, establishing it as the earliest regulator of osteoclastogenesis. Also, we showed that C/ebpα can protect mice against ovariectomy-induced bone loss in a mouse model of osteoporosis. Collectively, these results have established C/ebpα as a key transcriptional regulator of osteoclastogenesis as well as OC activity during postnatal development.

Materials and Methods

Generation of C/ebpα (f/f) LysM-Cre mice.

All animal studies were carried according to the legal requirements of the Association for Assessment and Accreditation of the Laboratory Animal Care International and the University of Alabama at Birmingham Institutional Animal Care and U4–8se Committee as well as the recommendations of the Animal Research: Reporting in Vivo Experiments guidelines. C/ebpα(f/f) mice (Jackson Laboratory, JAX no. 006447) (17,18) were crossed with LysM-Cre transgenic mice (Jackson Laboratory, JAX no. 004781) (19), and their progeny ($C/ebp\alpha^{flox/+/LysM\text{-}Cre}$) were bred to obtain C/ebpα (f/f) LysM-Cre mice. Mice were bred in-house and euthanatized by CO2 asphyxiation. Genotyping by PCR was carried out as described in a previous study (20). To detect floxed and excised bands, the products were amplified under the following conditions: 4 min at 94°C for initial denaturation followed by 35 cycles of 45 sec at 94°C, 30 sec at 60°C, and 1.5 min at 72°C, with a final round of 10 min at 72°C, in an ABI 2720 thermocycler. To detect Cre, the products were amplified under the following conditions: 1.5 min at 95°C for initial denaturation followed by 35 cycles of 30 sec at 94°C, 1 min at 67°C, and 2 min at 72°C, with a final round of 10 min at 72°C, in an ABI 2720 thermocycler. We used a 2% agarose gel for genotyping with DAPI in the loading buffer. Primers for genotyping have been listed in Table S1. All mice were maintained under a 12-hour light–dark cycle with ad libitum access to regular food and water at the UAB Animal Facility. Both male and female mutant and WT mice were randomly selected into group of five animals each. The investigators were not blinded during allocation, animal handling, and endpoint measurements.

Histological and Radiographic Procedures.

Preparation of tissue samples and histological analyses were performed as described previously (21,22). TRAP staining was performed to examine OC differentiation using a commercial kit (Sigma 387A-1KT) according to the instruction of the manufacturer. TRAP-positive multinucleated (more than 3 nuclei) cells were counted by light microscopy. Nonspecific esterase (NSE; Sigma 91A-1KT) staining was performed as described in previous studies (2,23,24). For X-ray analysis, radiography was performed using a high-resolution, soft X-ray system (Faxitron Model MX-20) by the UAB Small Animal Bone Phenotyping Core associated with the Center for Metabolic Bone Disease.

μ-CT Tomography.—Excised mouse humerus and femurs were scanned using the Scanco CT40 desktop cone-beam micro-CT scanner (Scanco Medical AG, Brüttisellen, Switzerland). The trabecular bone scanning was performed from the growth plate (310 slices at 12um per slice) analyzed using the CT Evaluation Program (v5.0A, Scanco Medical). The

scanning and analysis of the cortical bone were performed at the midshaft of the femur and consisted of 25 slices (12um per slice).

Histomorphometric Analysis.

Histomorphometric samples were non-decalcified hard-tissue sections processed as described (7,21). Briefly, for quantitative bone volume histomorphometry, 5-μm sections of C/ebpα (f/f) and C/ebpα (f/f) LysM-Cre mice were stained with Goldner's trichrome. For histomorphometric analysis of OC size and number, 10-μm sections of C/ebpα (f/f) and C/ebpα(f/f) LysM-Cre mice were TRAP stained without counterstaining. Histomorphometric analysis of these sections was performed using the NIH ImageJ program. In this analysis, we examined the following parameters: bone volume relative to tissue volume, the percentage of OC surface area to total bone surface area of the tibiae, the percentage of osteoblast surface area to total bone surface area of the tibiae, OC numbers per bone perimeter, osteoblast numbers per bone perimeter, distal hypertrophic growth plate thickness, proximal hypertrophic growth plate thickness, and trabecular thickness. Large multinucleated cells with cytoplasmic vesicles and intimate contact to bone were considered as OCs, and cuboidal mononuclear cells in intimate contact with osteoid or bone were identified as osteoblasts.

Mouse Bone Marrow (MBM) cells and OC-like cells.—MBM cells obtained from wild type and mutant mice as described (25,26) were cultured in α-MEM (Invitrogen) with 10% FBS (Invitrogen) containing M-CSF (20 ng/ml). After 1 day, cells were further cultured in the presence of 10 ng/ml RANKL (Peprotech) and M-CSF (10 ng/ml) to generate OCs.

Cell staining for F-actin Rings.—F-actin ring formation was evaluated as previously determine (27). In brief, cells were fixed with 3.7% formaldehyde and permeabilized with 0.2% Triton X-100. The cells were then blocked with 1% goat serum and 3% BSA and incubated with 2 U/ml rhodamine phalloidin (Molecular Probes) at room temperature for 20 min. The experiment was performed in a 24-well plate in duplicate on four independent occasions. For anti-Ctsk immunofluorescence stain, OCs on bovine bone slides were fixed by 4% formaldehyde, permeabilized with 0.2% Triton X-100, blocked with 5% goat serum and 100μg/ml unconjugated AffiniPure Fab Fragment Goat Anti-Mouse IgG (H+L) (Jackson ImmunoResearch Labs), incubated with mouse anti-mouse Ctsk primary antibody (1:100, Santa Cruz sc-48353) and then with FITC goat anti-mouse IgG (H+L) secondary antibody. Nuclei were visualized with 1μg/ml DAPI (4',6-diamidino-2-phenylindole; Sigma-Aldrich, D9542). Microscopy and 3-D construction by Imaris were performed as described (28).

Acridine Orange Staining—Acid production was determined using acridine orange as described previously (5). OCs were incubated in α-MEM containing 5 μg/ml of acridine orange (Sigma) for 15 min at 37°C, washed, and chased for 10 min in fresh media without acridine orange. The cells were observed under a fluorescence microscope with a 490 nm excitation filter and a 525 nm arrest filter. The experiment was performed in duplicate on four independent occasions in a 12 or 6-well plate.

***In vitro* Bone resorption Assays.—**Bone resorption activity was assessed as described (29–31). For scanning electron microscopy analysis, a consistent number of MBM cells were cultured on bovine cortical bone slices in 24-well plates stimulated by RANKL/M-CSF for 48 hours. 0.25 M ammonium hydroxide and mechanical agitation were utilized to remove cells adhering to the bone slices when the bone slices were harvested on day 6. Scanning electron microscopy (SEM) of bone slices was done using a Philips 515 SEM (Department of Materials Science and Engineering, UAB). Bone resorption pits were analyzed by WGA stain as described (32) with peroxidase-conjugated WGA-lectin (Sigma-Aldrich, L-3892) and DAB Peroxidase (HRP) Substrate Kit (Vector laboratories, SK-4100). The assays were performed in triplicate and presented as a representative observing area from each assay. Data quantification was achieved by measuring the percentage of the areas resorbed in three random resorption sites using ImageJ software from the National Institute of Health.

Immunostaining.—Immunostaining was carried out as described (7). Antibodies for C/ebpα, Acp5, Pu.1, c-Fos, and Nfatc1 were purchased from Santa Cruz Biotechnology (1:200 1:1000). Two specific antibodies, F4/80 (Biosource International) and CD11b (Pharmingen), were used as markers of monocyte/macrophage precursors as described previously (2,23). For the quantification of immunofluorescence, we used NIH image software (ImageJ) to perform counts and the percent of positive cells represents the number of positive cells expressed the targeted gene divided by TRAP-positive cells.

Real-time quantitative PCR (qPCR) and Semi-quantitative PCR.—RNA samples were obtained from C/ebpα (f/f) and C/ebpα (f/f) LysM-Cre MBM cultured with M-CSF/RANKL, or from transduced pBMN-C/ebpα MBM with TRIzol reagent (Life Technologies, 15596018). TaqMan probes purchased from Applied Biosystems as listed in Table S2 were utilized in qPCR which was performed as described (33,34). Briefly, cDNA were amplified by Fast SYBR Green Master Mix (5mL) P/N 4385612 (Applied Biosystems). Step-One real-time PCR system (Applied Biosystems) was used to detect fluorescence from each TaqMan probe using the TaqMan Gene Expression assays (Life Technologies, Applied Biosystems) or SYBR Green reagents (Life Technologies, 4385610). The mRNA expression levels were normalized against the housekeeping gene hypoxanthine-guanine phosphoribosyl transferase (Hprt). Primer sequences used for semi-quantitative PCR are listed in Table S2. PCR conditions are available upon request. Experiments were repeated at least three times.

Western blot Analysis.—Western blotting was performed as described (35). To examine protein expression, gel images were captured, and results were visualized by Fluor-S Multi-Imager, then quantified by Multi-Analyst software (Bio-Rad). Antibodies for C/ebpα, Pu.1, c-Fos, Nfatc1 were purchased from Santa Cruz Biotechnology; and anti-cathepsin K antibody was used as described above. Results were normalized against housekeeping protein glyceraldehyde-3-phosphate dehydrogenase (GAPDH).

Chromatin Immunoprecipitation.—Ctsk (−4000/+301) promoter region was analyzed with PROMO3.0 (http://alggen.lsi.upc.es/) using version 8.3 of the TRANSFAC database for putative C/ebpα binding sites. ChIP was performed using monoclonal anti-C/ebpα antibody

(sc-61X, Santa Cruz Biotechnology). Subsequently, DNA was extracted and qPCR was performed as described (36,37). The DNA was prepared from MBM induced by RANKL and M-CSF for three days using the following primers in the promoter regions of Ctsk listed in Table S3.

Promoter Analyses.—Ctsk promoter was amplified using PCR from BAC clones provided by the BACPAC Resource Center at Children's Hospital Oakland Research Institute. The amplified fragments were cleaved and ligated into the pGL3 vector (Promega). RAW 264.7 cells were cultured in osteogenic medium (no FBS for 5d), re-seeded on 96-well plates, and cotransfected with 100ng/well of each construct as well as 50ng/well of pSV–β-galactosidase construct and incubated for 6–8 h. The culture medium was replaced with osteogenic medium and cultured for 2 days. The macrophage RAW264.7 cells were induced by RANKL and M-CSF for 2 days to promote the formation of multinucleated OCs, which was then followed by transfection with the corresponding luciferase reporter vectors. Luciferase activity was measured using a Steady-Glo luciferase assay system (Promega cat. no. E2510). pSV–β-galactosidase activity was measured using a β-galactosidase Enzyme Assay system (Promega cat. no. E2000) and normalized against β-galactosidase activity as described (7,33).

Ovariectomy (OVX) Procedure.

C/ebpα$^{f/f}$LysM-Cre and C/ebpα$^{f/f}$ mice were either dorsal ovariectomized or sham-operated (sham) under anesthetization with a mixture of ketamine:xylazine (80:10 mg/kg) as described (38). Mutant and wild-type mice were compared with Sham or OVX mice (OVX), respectively. At four weeks post-operation, femurs and uteri were harvested for phenotypic and radiological analysis as previously described.

Statistical Analysis.

Experimental data are reported as mean±SD of triplicate independent samples with male and female mice in each group. Data were analyzed with the Student's t-test or two-way analysis of variance using GraphPad Prism statistical program. P values <0.05 were considered significant. *, $P < 0.05$;**, $P < 0.01$ (throughout the paper). Error bars depict SD.

Results

C/ebpα$^{f/f}$LysM-Cre mice display an osteopetrotic phenotype.

To overcome the early lethality of the *C/ebpα*$^{-/-}$ mice, a monocyte-specific C/ebpα-deficient mouse model was generated by crossing *C/ebpα*$^{f/f}$ mice with LysM-Cre mice to generate C/ebpα$^{f/f}$LysM-Cre mice, and the genotypes were confirmed by PCR analysis (Fig. 1A). Compared to wild-type (WT) mice, the *C/ebpα*$^{f/+}$LysM-Cre mice and *C/ebpα*$^{f/f}$ showed no overt bone phenotype. As such, the WT, *C/ebpα*$^{f/+}$LysM-Cre mice and C/ebpα$^{f/f}$ were used as controls in the study. Femoral radiograph analysis at 14 and 24 weeks of age showed that the increase in bone density in the C/ebpα$^{f/f}$LysM-Cre mice accentuated as the mice aged (Fig. 1B, C). We noted that both female and male *C/ebpα*$^{f/f}$LysM-Cre mice displayed similar bone phenotypes as compared to the control mice, indicating that the defect in bone density observed in the mutant mice was not sex-specific. Accordingly,

micro-CT (μ-CT) analysis of the distal femora of male and female at 14 weeks of age showed a significant increase in both trabecular and cortical bone density in the *C/ebpα*$^{f/f}$LysM-Cre mice as compared to WT controls (Fig. 1D). Quantitative μ-CT analysis further confirmed that C/ebpα$^{f/f}$LysM-Cre mice showed significant increases in bone volume/trabecular volume, trabecular number and trabecular thickness, but a significant decrease in trabecular separation, as well as a significant increase in cortical bone density (Fig. 1E). To assess the onset, progression and severity of osteopetrosis in *C/ebpα*-deficient mice, we examined the bone phenotype of both mutant and wild-type mice at various stages of skeletal development (Suppl. Fig. 1). Postnatal C/ebpα$^{f/f}$LysM-Cre mice (i.e. 1, 2 weeks) exhibited enhanced bone radiodensity (Suppl. Fig. 1A, B) while bone radiographs and quantitative aging data from older C/ebpα$^{f/f}$LysM-Cre mice (i.e. 14 and 16 weeks) showed worsening osteopetrosis (Suppl. Fig. 1C, D). These results indicated that the conditional deletion of C/ebpα in the monocyte cell lineage caused an abnormally dense bone.

C/ebpα$^{f/f}$LysM-Cre mice display an osteopetrotic phenotype due to impaired OC and macrophage development.

Hematoxylin and Eosin (H&E) staining of femoral sections form newborn *C/ebpα*$^{f/f}$LysM-Cre mice showed significantly increased trabecular bone as compared with age-matched C/ebpα$^{f/f}$ littermates (Fig. 2A). However, the bone collars lined with osteoblasts were comparable in *C/ebpα*$^{f/f}$LysM-Cre and *C/ebpα*$^{f/f}$ mice (Fig. 2A, black arrows). Further H&E staining at 14 weeks showed higher bone density in the mutant mice as compared to age-matched C/ebpα$^{f/f}$ littermates; further indicating that the bone density of the mutant mice exacerbated with aging (Fig. 2B). Consistently, Goldner's Trichrome staining confirmed a dramatic increase in mineralized tissue in the *C/ebpα*$^{f/f}$LysM-Cre mice at 14 week as compared to C/ebpα$^{f/f}$ mice (Fig. 2C). Accordingly, *C/ebpα*$^{f/f}$LysM-Cre mice showed a significant increase in bone volume per trabecular volume, trabecular thickness, and trabecular number, but a decrease in trabecular space as compared to control littermates (Fig. 2D). Whereas the mutant mice showed no overt defect in osteoblast development, the mutant had a significant decrease in OC number per bone surface as compared to *C/ebpα*$^{f/f}$ (Fig. 2D). Given that OC originates from the monocyte/macrophage cell lineage, we next examined the effect of *C/ebpα* on the development of OC precursors as well as OC lineage priming (Fig 2E, F). Flow cytometric analysis showed that the *C/ebpα* CKO exhibited decreased macrophage development (i.e. CD11b+F4/80+ cells) by almost 30% (Fig. 2E). Moreover, conditional *C/ebpα* deletion significantly affected the number of CD11b +CD115+ pre-OCs (decreased by 70%) (Fig. 2F), suggesting a block in the OC lineage priming. The data indicated that C/ebpα deletion in the monocyte cell lineage caused osteopetrosis by impairing OC development.

LysM-Cre mediated C/ebpα deletion impairs OC differentiation and activity *in vitro*.

Next, we examined the abilities of *C/ebpα*-deficient OC precursors to differentiate into functional OCs through stimulation by M-CSF and RANKL (Fig. 3). Our previous study demonstrated the key role of C/ebpα in OC differentiation *in vitro* through rescue experiments conducted after shRNA-induced gene silencing (39). Mouse bone marrow (MBM) cells, widely used as primary OC precursors, were isolated from *C/ebpα*$^{f/f}$LysM-Cre and *C/ebpα*$^{f/f}$ mice and then treated with M-CSF and RANKL for 5 days to promote OC

differentiation (Fig. 3). Whereas WT cells formed numerous OCs as examined by TRAP staining (Fig. 3A lower panel and Suppl. Fig. 2A), the ability of C/ebpα-deficient MBM cells to differentiate into OC was reduced by almost 50 percent (Fig. 3A,F and Suppl. Fig. 2C). Notably, nonspecific esterase staining of the induced MBM showed a 30-percent reduction in the number of positive cells, confirming a mild defect in monocyte/macrophage development (Suppl. Fig. 2B, C). This is consistent with previous analysis (Fig. 2E–G). Provided the remaining OCs are functional, a 50-percent reduction in OC number will be able to maintain bone integrity. But based on the osteopetrosis exhibited by mutant mice, it is highly possible that C/ebpα also plays an indispensable yet independent role in OC function. Therefore, we examined the effect of the C/ebpα deletion on actin ring formation, an important feature of mature OCs, and extracellular acidification, critical for OC function. We found that the C/ebpα deletion significantly impaired extracellular acidification (Fig. 3A upper panel, E) and also significantly reduced actin ring formation (Fig. 3B, upper panel). For further bone resorption assays, a consistent number of mutant and wild-type OCs were seeded on bovine cortical bone slices in 24-well plates. Unlike the well polarized F-actin rings in *C/ebpα*$^{f/f}$ control, we found significantly impaired actin ring formation on bone slice seeded by C/ebpα-deficient OCs (Fig. 3B, lower panel). Consistently with the posture, bone resorption analysis by WGA staining (Fig. 3C, G) and SEM (Fig. 3D, H) demonstrated that the C/ebpα deletion inhibited osteoclastic bone resorption. These results indicated that the lack of C/ebpα severely affected OC differentiation and function leading to inhibition of osteoclastic bone resorption.

C/ebpα deletion represses gene associated with OC differentiation and function *in vivo*.

In investigating the molecular basis of *C/ebpα* deletion on early and late states of OC development, we examined the expressions of OC marker genes by immunostaining of paraffin sections of newborn *C/ebpα*$^{f/f}$LysM-Cre mice as compared to WT controls, counting only TRAP-positive cells expressing the protein of interest (Fig. 4). Our immunostaining confirmed that *C/ebpα* was effectively ablated (Fig. 4A,G) and OC number was significantly reduced, through analysis of TRAP staining, in the *C/ebpα*$^{f/f}$LysM-Cre mice as compared to *C/ebpα*$^{f/f}$ mice (Fig. 4F,G). Interestingly, the Nfatc1 target gene Ctsk was repressed in *C/ebpα*$^{f/f}$LysM-Cre mice (Fig. 4B, G). Consistent with the decreased OC development, *C/ebpα* deletion significantly repressed c-Fos (Fig. 4C,G) and Pu.1 (Fig. 4D,G), critical for the commitment of bone marrow macrophages to the OC lineage (1) as compared to *C/ebpα*$^{f/f}$ mice. Moreover, the *C/ebpα*$^{f/f}$LysM-Cre mice showed significantly reduced expression of Nfatc1 (Fig. 4E, G) critical for OC lineage priming as well as terminal OC differentiation. The results indicate that the conditional deletion of the C/ebpα in the monocyte cell lineage impaired OC development by repressing genes associated with OC differentiation and function.

Monocyte-specific C/ebpα deletion inhibited the expression of genes associated with OC differentiation and function *in vitro*.

We further confirmed these findings by examining the expressions of the OC marker genes from the mutant and WT mice by both qPCR and Western blotting (Fig.5). Consistently, our Western blotting analysis confirmed that C/ebpα protein levels were significantly reduced in the *C/ebpα*$^{f/f}$LysM-Cre mice. Moreover, the c-Fos, Nfatc1, Ctsk, and Atp6i protein levels

were significantly repressed in the *C/ebpα*$^{f/f}$LysM-Cre mice as compared to the *C/ebpα*$^{f/f}$ mice (Fig. 5A, B). We confirmed that the C/ebpα mRNA level was significantly repressed in the *C/ebpα*$^{f/f}$LysM-Cre mice as compared to control *C/ebpα*$^{f/f}$ mice (Fig. 5C). Consistently, we showed that the mRNA levels of c-Fos, Nfatc1, and Ctsk as well as selected OC genes critical for cell function (Mmp9, Atp6i, and Calcr) were significantly repressed in the *C/ebpα*$^{f/f}$LysM-Cre mice (Fig. 5C). However, while our Western blotting analysis demonstrated that the C/ebpα deletion led to a 3-fold decrease in Pu.1 protein levels (Fig. 5A, B), our data also showed that C/ebpα deletion showed no effect on Pu.1 mRNA levels (Fig. 5C). We noted that the C/ebpα conditional deletion decreased Ctsk, c-Fos, ATP6i, and Nfatc1 protein levels by 2.5, 2.5, 5, and 2.6 fold, respectively (Fig. 5B), which was associated with a reduced mRNA levels by 2.5, 1.5, 2.5, and 3 fold, respectively (Fig. 5C). This analysis indicated that C/ebpα deficiency significantly repressed the expression of OC genes at the transcriptional level which translated into decreased protein levels. The results indicate that C/ebpα deletion impairs OC differentiation and function by repressing gene expression at the transcriptional level.

C/ebpα silencing reduced OC differentiation as well as OC function *in vitro*.

C/ebpα was excised in C/ebpα$^{f/f}$ MBM through Adenovirus-Cre vector for *in vitro* OC differentiation analysis along with a Scramble control, most efficiently in early stages (within day 1) of osteoclastogenic induction (Suppl. Fig. 3A,B). TRAP staining showed a significant decrease in osteoclastogenesis and OC fusion in the C/ebpα deficient cells induced by RANKL (Suppl. Fig. 3C). In addition, we analyzed actin ring formation by immunostaining which showed that the formation of F-actin rings was severely defective in the C/ebpα-deficient cells at 24 and 48 hours (Suppl. Fig. 3D, E). Interestingly, at 72 hours, when MBM had already differentiated into multinucleated OCs before being transfected with a Adenovirus-Cre vector, the TRAP activity of ad cre-transfected OCs has significantly reduced, and F-actin ring were also disrupted and significantly reduced compared to scramble control, indicating impaired OC polarization and function (Suppl. Fig. 3D, E). The results further establish a critical role for C/ebpα in OC differentiation and function.

C/ebpα directly upregulates Ctsk expression by associating with its promoter.

We previously reported that the sequence between −51 and −34 within the pCCAT-137 construct contains a *Ctsk* CCRE in which internal deletion induced a total loss of Ctsk activity, which was found to be a *C/ebpα* binding site (TTCCGCAAT) (33). Nevertheless, it has been suspected that there might be more binding sites for *C/ebpα* on the *Ctsk* promoter. In order to further examine whether *C/ebpα* has additional binding sites on the Ctsk promoter (−4000/+301), chromatin immunoprecipitation (ChIP) assay was performed using DNA prepared from MBM cells induced by M-CSF and RANKL for 4 days as described (36,37). DNA was pulled down, amplified, and analyzed using primers shown in Fig. 6A. The ChIP input value using each primer represents the binding efficiency of an adjacent region around the location of the primer pair. We found several C/ebpα binding sites on the Ctsk promoter region (−4000/+301) (Fig. 6B). We discovered that C/ebpα/Ctsk primer pair 5 resulted in the highest amplification followed by significant amplification resulting from primer pair 4, indicating that these C/ebpα binding sites on these Ctsk promoter regions are the most efficient (Fig. 6B). Our subsequent luciferase assay showed highest activity in the

longest Ctsk promoter fragments (−2445/+301), which still remained with the (−2232/+301), (−1825/+301), and (−1630/+301) fragments, suggesting critical C/ebpα binding sites at −1141 and −1030 in addition to the known binding site at −47 (33) (Fig. 6C). Notably, the (−1630/+301) fragment retained approximately 80% of the luciferase activity of the longest fragment, which is a significantly higher percentage than that of the (−459/+301) and (−717/+301) fragments, thereby suggesting the presence of an important enhancer in addition to the previously reported CCRE at −47 (Fig. 6C). The results demonstrated that C/ebpα directly associated with the Ctsk promoter to upregulate Ctsk, further establishing it as a key transcriptional regulator of OC differentiation, activation, and function through direct transcriptional gene regulation.

C/ebpα$^{f/f}$LysM-Cre mice exhibit protection against ovariectomy-induced bone loss.

In order to examine how C/ebpα regulates bone remodeling under pathological states, we performed sham surgery and ovariectomy (OVX) on C/ebpα$^{f/f}$ and C/ebpα$^{f/f}$LysM-Cre mice. The OVX mouse model mimics estrogen-depletion-induced bone loss in postmenopausal women, and provide an important mouse model to study the role of C/ebpα in bone loss induced estrogen deprivation. Four weeks following the operations, mouse body and uterine sizes were examined to confirm the effects of OVX in C/ebpα$^{f/f}$LysM-Cre and C/ebpα$^{f/f}$ mice (Fig. 7A, B). Uteri in OVX-C/ebpα$^{f/f}$ and OVX-C/ebpα$^{f/f}$LysM-Cre had dramatically decreased in size compared to that in post-sham C/ebpα$^{f/f}$ mice (Fig. 7B). Radiographic images revealed that, while OVX-C/ebpα$^{f/f}$ mice exhibited severe OVX-induced bone loss, OVX-C/ebpα$^{f/f}$LysM-Cre femurs conversely showed an enhanced bone density compared to the control femurs (Fig. 7C, D). To further explore the bone phenotypes of OVX-mutant mice, μCT analysis was performed on mouse femurs at 4 weeks post operation (Fig. 7E). Sham-C/ebpα$^{f/f}$LysM-Cre retained significantly higher bone density compare to sham-C/ebpα$^{f/f}$. Furthermore, when compared to OVX-C/ebpα$^{f/f}$ control group, quantification analysis of the distal femora showed increased bone volume/tissue volume and trabecular number in OVX-C/ebpα$^{f/f}$LysM-Cre mice which was comparable to that of the sham-C/ebpα$^{f/f}$LysM-Cre (Fig. 7F). The results indicate that C/ebpα deficiency protects mice from OVX-induced bone loss.

Discussion

The role of C/ebpα in postnatal skeletal development and bone homeostasis have not been studied since newborn C/ebpα null mice die within several hours after birth. Hence, this study provides significant insights into the role of *C/ebpα* as a key regulator of OC differentiation and function, under physiological and pathological condition, beyond its known functions in regulating cell lineage commitment. We revealed that *C/ebpα* directly regulates *CtsK* gene expression thereby resulting in OC differentiation and function and mildly defective macrophage development.

The molecular basis underlying *C/ebpα* control of the cascade of transcription factors that specify OC terminal differentiation, including cell activation and function.

C/ebpα is an important transcriptional regulator of hematopoiesis, which acts through its ability to bind DNA and influence transcriptional activities of various genes. Recent studies

thus far have exclusively argued for the importance of *C/ebpα* in monocyte/macrophage and OC lineage allocation (15,40). Notably, our previous *in vitro* gain-of-function and loss-of-function studies have indicated that C/ebpα functions throughout osteoclastogenesis, and potentially, in OC function (41). In this study, we found that *in vivo* OC terminal differentiation in C/ebpα CKO mice was affected along with severely impaired osteoclastic bone resorption, which suggests that C/ebpα might play a critical yet independent role in OC terminal differentiation. However, the mechanisms underlying the role of *C/ebpα* in postnatal physiological and pathological skeletal development remain elusive. Since *C/ebpα* can be removed through an ubiquitin-proteasome system-mediated mechanism (42), it is possible that RANKL protects *C/ebpα* from being degraded, thereby leading to its high expression in the cytoplasm during osteoclastogenic induction; leading to upregulated expressions of *Nfatc1* and *c-fos* to induce OC lineage commitment, which precedes OC differentiation and function. Notably, *C/ebpα* also directly up-regulates OC genes (e.g. *Ctsk* and *Atp6i*), which contributes to OC-mediated bone resorption involving actin ring formation, extracellular acidification and matrix protein degradation. Hence, deficiency of *C/ebpα* can suppress the expression of these regulating factors and function genes, resulting in osteopetrosis. Interestingly, Pu.1 protein levels, but not its mRNA level, in C/ebpα$^{f/f}$LysM-Cre was downregulated. We have previously shown that constitutive C/ebpα ablation significantly reduced Pu.1 expression at both protein and mRNA levels indicating C/ebpα could play major roles in terminal OC differentiation and that there might be a post-translational mechanism that accounts for the differential Pu.1 gene expression profile in OCs (33). It is also possible that in OCs, C/ebpα interacts and forms multiprotein complexes with other coactivators to induce gene expression and post-translational changes that is specific to OC function. On the other hand, c-Fos (a key regulator of OC-macrophage lineage determination) is significantly downregulated in *C/ebpα$^{f/f}$LysM-Cre* suggesting an important role for c-Fos at different stages throughout OC development due to direct interactions with two C/ebpα binding sites in the promoter region of c-Fos (33).

C/ebpα plays a key role in monocyte/macrophage development and OC differentiation while also regulating OC function and thereby mediating bone resorption.

In differentiating from their hematopoietic precursors, OC undergoes a robust process of lineage determination and cell maturation before committing to terminal differentiation in which OC activation and function take place, allowing for further investigation of later differentiation stage (43). In this study, we examined the effects that conditional loss of C/ebpα using LysM-Cre in myeloid precursor cells using a variety of parameters. The gene knockout strategies using the macrophage-specific LysM-Cre might result in incomplete C/ebpα knockout in mouse mature OCs (44); potentially affecting the presentation of osteopetrosis in mutant mice. To overcome this challenge, we had examined a large number of both male and female mice, as well as utilized the Ad-Cre lentiviral approach to knock out C/ebpα gene *in vitro* for further OC differentiation and function assays. We revealed that C/ebpα CKO impaired actin ring formation, inhibited extracellular acidification, and decreased osteoclastic bone resorption, and that monocyte/macrophage development was repressed (Fig. 3, Suppl. Fig. 3). Moreover, our flow cytometry data demonstrated that C/ebpα deletion in monocyte/macrophages significantly altered the abundance of OCs (reduced by more than 70 percent) while reducing the number of the myeloid precursors (ie.

macrophages) by only 30 percent (Fig. 2E–G), suggesting either that C/ebpα is directly involved in regulating the proliferation and function of macrophages and/or that its regulation also occurs at a much later stage in OC lineage commitment. Provided the remaining OCs are functional, a 50-percent reduction in OC number will be able to maintain bone integrity (Fig. 3F). But based on the osteopetrosis exhibited by mutant mice, it is highly possible that C/ebpα also plays an indispensable yet independent role in OC function. Furthermore, when comparing the bone slices seeded with the same number of WT and mutant OCs, the numbers of induced cells were in fact similar despite the disrupted actin ring indicating nonfunctional OCs (Fig. 3B). The bone resorption defects were further confirmed by subsequent WGA and electron microscopy analyses. Pertaining to the lack of TRAP+ cells in C/ebpα CKO mice, since C/ebpα also plays a role in early osteoclastogenesis and other cells of the hematopoietic origin, the loss of C/ebpα in monocyte through LysM-Cre CKO impaired monocyte and early OC differentiation, potentially leading to the decrease in TRAP+ cells. It would be interesting in future studies to determine the exact mechanisms by which C/ebpα regulate monocyte/macrophage development as macrophages have major functions in many inflammatory conditions.

C/ebpα may be able to exert its regulatory effects on critical OC regulator genes and OC function genes to selectively alter the activation and function stages in normal OC development.

Direct interaction with C/ebpα binding sites as a CCRE in the Ctsk promoter region could also be the mechanism underlying the effects of C/ebpα on OC function (33). This interaction, despite being predominant in early stages of osteoclastogenesis, might still retain significant influences throughout OC differentiation maturation, activation, and function in postnatal bone homeostasis. Furthermore, it is likely that the critical C/ebpα binding sites at −1141 and −1030 in addition to the known binding site at −47 in the Ctsk promoter region could also play important regulatory roles in OC activity (Fig. 6). This pathway underscores another possibility pertaining to C/ebpα's control of the cascade of transcription factors that specifies postnatal OC activation and function. C/ebpα might directly and potently bind to the promoter regions of c-Fos and Ctsk to exert its regulatory effects and thereby promote OC function. Through directly upregulating the expressions of OC transcription factors and key OC function genes, C/ebpα may play an indispensable role in upregulating the expression of important OC-specific genes, which further promotes postnatal OC activation and function. Taken together, our findings strongly suggest that C/ebpα plays a major regulatory role in OC activation and function beyond its known functions in OC lineage commitment and differentiation.

C/ebpα may be new target for the development of future novel and effective treatments for osteolytic diseases.

Osteoporosis is a chronic condition characterized by abnormally high bone resorption along with diminishing bone formation, which potentially results in decreased bone strength and increased risk of bone fracture. Bone fragility associated with osteoporosis can lead to severe disability and even early mortality. Notably, bone loss in women rapidly increases after menopause due to lower levels of estrogen. Despite the significant effort that has been invested in past several decades, current treatment options are constrained by lower response

rates and adverse side-effects. This study not only improves our understanding of the role of transcription factors in OC differentiation, activation, and function, but it may also facilitate the development of novel treatments for osteolytic diseases, including osteoporosis. C/ebpα is an endogenous regulator that plays a key role in OC activation and function. C/ebpα deficiency in OCs completely protected mice against OVX-induced bone loss (Fig. 7). Thus, C/ebpα is an effective bone disease target and C/ebpα inhibitors may lead to desirable therapeutics and further optimize the current treatment options for local bone loss in periodontal disease and osteoarthritis. However, screening for effective C/ebpα inhibitors can be problematic in systemic osteolytic disorders, such as osteoporosis, due to the fact that C/ebpα is ubiquitously expressed and involved in proliferation arrest and the differentiation of multiple cell types. In order to overcome these limitations, it is important to further explore the mechanisms underlying how C/ebpα specifically regulates osteoclastogenesis OC differentiation, activation and function and to reveal effective upstream C/ebpα regulators that are specific to OCs. Although our work may not result in new osteoporosis therapies currently or directly, the characterization of the mechanism underlying how C/ebpα regulates OC differentiation, activation, and function will provide important mechanistic insights into OC biology that can greatly benefit future research in the investigation of potential C/ebpα regulators, as well as pointing to a new target for the development of novel and effective treatments for osteolytic diseases.

Supplementary Material

Refer to Web version on PubMed Central for supplementary material.

Acknowledgements

We thank Ms. Diep Nguyen, Ms. Christie Paulson, and Ms. Abigail McVicar for their assistance with the manuscript; and Dr. Matthew McConnell for the bioinformatics analysis assistance. We appreciate the assistance of The UAB Center for Metabolic Bone Disease (P30 AR046031). We also appreciate the assistance of the Comprehensive Flow Cytometry Core at UAB (P30 AR048311).We are also grateful for the assistance of the Small Animal Phenotyping Core, Metabolism Core, and Neuroscience Molecular Detection Core Laboratory at UAB (P30 NS0474666). This work was supported by National Institutes of Health [AR-44741 and DE-023813 to Y.P.L. and AR-070135 to W.C.]

References

1. Boyle WJ, Simonet WS, Lacey DL 2003 Osteoclast differentiation and activation. Nature 423(6937):337–342. [PubMed: 12748652]
2. Takayanagi H, Kim S, Koga T, Nishina H, Isshiki M, Yoshida H, Saiura A, Isobe M, Yokochi T, Inoue J, Wagner EF, Mak TW, Kodama T, Taniguchi T 2002 Induction and activation of the transcription factor NFATc1 (NFAT2) integrate RANKL signaling in terminal differentiation of osteoclasts. Developmental cell 3(6):889–901. [PubMed: 12479813]
3. Feng X, McDonald JM 2011 Disorders of Bone Remodeling. Annual review of pathology 6:121–145.
4. Li YP, Chen W, Stashenko P 1996 Molecular cloning and characterization of a putative novel human osteoclast-specific 116-kDa vacuolar proton pump subunit. Biochemical and biophysical research communications 218(3):813–821. [PubMed: 8579597]
5. Li YP, Chen W, Liang Y, Li E, Stashenko P 1999 Atp6i-deficient mice exhibit severe osteopetrosis due to loss of osteoclast-mediated extracellular acidification. Nature genetics 23(4):447–451. [PubMed: 10581033]

6. Li YP, Alexander M, Wucherpfennig AL, Yelick P, Chen W, Stashenko P 1995 Cloning and complete coding sequence of a novel human cathepsin expressed in giant cells of osteoclastomas. Journal of bone and mineral research : the official journal of the American Society for Bone and Mineral Research 10(8):1197–1202.
7. Chen W, Yang S, Abe Y, Li M, Wang Y, Shao J, Li E, Li YP 2007 Novel pycnodysostosis mouse model uncovers cathepsin K function as a potential regulator of osteoclast apoptosis and senescence. Human molecular genetics 16(4):410–423. [PubMed: 17210673]
8. Ramji DP, Foka P 2002 CCAAT/enhancer-binding proteins: structure, function and regulation. Biochemical Journal 365(Pt 3):561–575. [PubMed: 12006103]
9. Friedman AD 2015 C/EBPalpha in normal and malignant myelopoiesis. International journal of hematology 101(4):330–341. [PubMed: 25753223]
10. Ohlsson E, Schuster MB, Hasemann M, Porse BT 2016 The multifaceted functions of C/EBPalpha in normal and malignant haematopoiesis. Leukemia 30(4):767–775. [PubMed: 26601784]
11. Bueno C, Sardina JL, Di Stefano B, Romero-Moya D, Munoz-Lopez A, Ariza L, Chillon MC, Balanzategui A, Castano J, Herreros A, Fraga MF, Fernandez A, Granada I, Quintana-Bustamante O, Segovia JC, Nishimura K, Ohtaka M, Nakanishi M, Graf T, Menendez P 2016 Reprogramming human B cells into induced pluripotent stem cells and its enhancement by C/EBPalpha. Leukemia 30(3):674–682. [PubMed: 26500142]
12. Di Stefano B, Collombet S, Jakobsen JS, Wierer M, Sardina JL, Lackner A, Stadhouders R, Segura-Morales C, Francesconi M, Limone F, Mann M, Porse B, Thieffry D, Graf T 2016 C/EBPalpha creates elite cells for iPSC reprogramming by upregulating Klf4 and increasing the levels of Lsd1 and Brd4. Nature cell biology 18(4):371–381. [PubMed: 26974661]
13. Friedman AD 2007 C/EBPalpha induces PU.1 and interacts with AP-1 and NF-kappaB to regulate myeloid development. Blood cells, molecules & diseases 39(3):340–343.
14. Kasakura K, Takahashi K, Itoh T, Hosono A, Nunomura S, Ra C, Momose Y, Itoh K, Nishiyama C, Kaminogawa S 2014 C/EBPα controls mast cell function. FEBS Letters 588(24):4645–4653. [PubMed: 25447519]
15. Feng R, Desbordes SC, Xie H, Tillo ES, Pixley F, Stanley ER, Graf T 2008 PU.1 and C/EBPalpha/beta convert fibroblasts into macrophage-like cells. Proceedings of the National Academy of Sciences of the United States of America 105(16):6057–6062. [PubMed: 18424555]
16. Schuster MB, Porse BT 2009 C/EBPalpha in leukemogenesis: identity and origin of the leukemia-initiating cell. BioFactors (Oxford, England) 35(3):227–231. [PubMed: 19322763]
17. Welner RS, Bararia D, Amabile G, Czibere A, Benoukraf T, Bach C, Wansa KD, Ye M, Zhang H, Iino T, Hetherington CJ, Akashi K, Tenen DG 2013 C/EBPalpha is required for development of dendritic cell progenitors. Blood 121(20):4073–4081. [PubMed: 23547051]
18. Zhang DE, Zhang P, Wang ND, Hetherington CJ, Darlington GJ, Tenen DG 1997 Absence of granulocyte colony-stimulating factor signaling and neutrophil development in CCAAT enhancer binding protein alpha-deficient mice. Proceedings of the National Academy of Sciences of the United States of America 94(2):569–574. [PubMed: 9012825]
19. Clausen BE, Burkhardt C, Reith W, Renkawitz R, Forster I 1999 Conditional gene targeting in macrophages and granulocytes using LysMcre mice. Transgenic research 8(4):265–277. [PubMed: 10621974]
20. Growney JD, Shigematsu H, Li Z, Lee BH, Adelsperger J, Rowan R, Curley DP, Kutok JL, Akashi K, Williams IR, Speck NA, Gilliland DG 2005 Loss of Runx1 perturbs adult hematopoiesis and is associated with a myeloproliferative phenotype. Blood 106(2):494–504. [PubMed: 15784726]
21. Yang S, Li YP 2007 RGS10-null mutation impairs osteoclast differentiation resulting from the loss of [Ca2+]i oscillation regulation. Genes & development 21(14):1803–1816. [PubMed: 17626792]
22. Yang S, Hao L, McConnell M, Zhou X, Wang M, Zhang Y, Mountz JD, Reddy M, Eleazer PD, Li Y- P, Chen W 2013 Inhibition of Rgs10 Expression Prevents Immune Cell Infiltration in Bacteria-induced Inflammatory Lesions and Osteoclast-mediated Bone Destruction. Bone Research 1(3): 267–281. [PubMed: 24761229]
23. Chen W, Li YP 1998 Generation of mouse osteoclastogenic cell lines immortalized with SV40 large T antigen. Journal of bone and mineral research : the official journal of the American Society for Bone and Mineral Research 13(7):1112–1123.

24. Henkel GW, McKercher SR, Leenen PJ, Maki RA 1999 Commitment to the monocytic lineage occurs in the absence of the transcription factor PU.1. Blood 93(9):2849–2858. [PubMed: 10216079]
25. Kelly KA, Tanaka S, Baron R, Gimble JM 1998 Murine bone marrow stromally derived BMS2 adipocytes support differentiation and function of osteoclast-like cells in vitro. Endocrinology 139(4):2092–2101. [PubMed: 9528998]
26. Kurland JI, Kincade PW, Moore MA 1977 Regulation of B-lymphocyte clonal proliferation by stimulatory and inhibitory macrophage-derived factors. The Journal of experimental medicine 146(5):1420–1435. [PubMed: 303681]
27. Feng S, Deng L, Chen W, Shao J, Xu G, Li YP 2009 Atp6v1c1 is an essential component of the osteoclast proton pump and in F-actin ring formation in osteoclasts. The Biochemical journal 417(1):195–203. [PubMed: 18657050]
28. Yang DQ, Feng S, Chen W, Zhao H, Paulson C, Li YP 2012 V-ATPase subunit ATP6AP1 (Ac45) regulates osteoclast differentiation, extracellular acidification, lysosomal trafficking, and protease exocytosis in osteoclast-mediated bone resorption. Journal of bone and mineral research : the official journal of the American Society for Bone and Mineral Research 27(8):1695–1707.
29. Gao B, Chen W, Hao L, Zhu G, Feng S, Ci H, Zhou X, Stashenko P, Li YP 2013 Inhibiting periapical lesions through AAV-RNAi silencing of cathepsin K. Journal of dental research 92(2): 180–186. [PubMed: 23166044]
30. Ma J, Chen W, Zhang L, Tucker B, Zhu G, Sasaki H, Hao L, Wang L, Ci H, Jiang H, Stashenko P, Li YP 2012 RNAi mediated silencing of Atp6i prevents both periapical bone erosion and inflammation in the mouse model of endodontic disease. Infection and immunity
31. Ma J, Chen W, Zhang L, Tucker B, Zhu G, Sasaki H, Hao L, Wang L, Ci H, Jiang H, Stashenko P, Li YP 2013 RNA interference-mediated silencing of Atp6i prevents both periapical bone erosion and inflammation in the mouse model of endodontic disease. Infection and immunity 81(4):1021–1030. [PubMed: 23166162]
32. Zhao H, Ito Y, Chappel J, Andrews NW, Teitelbaum SL, Ross FP 2008 Synaptotagmin VII regulates bone remodeling by modulating osteoclast and osteoblast secretion. Developmental cell 14(6):914–925. [PubMed: 18539119]
33. Chen W, Zhu G, Hao L, Wu M, Ci H, Li YP 2013 C/EBPalpha regulates osteoclast lineage commitment. Proceedings of the National Academy of Sciences of the United States of America 110(18):7294–7299. [PubMed: 23580622]
34. Wu M, Chen W, Lu Y, Zhu G, Hao L, Li YP 2017 Galpha13 negatively controls osteoclastogenesis through inhibition of the Akt-GSK3beta-NFATc1 signalling pathway. Nature communications 8:13700.
35. Yang S, Wei D, Wang D, Phimphilai M, Krebsbach PH, Franceschi RT 2003 In vitro and in vivo synergistic interactions between the Runx2/Cbfa1 transcription factor and bone morphogenetic protein-2 in stimulating osteoblast differentiation. Journal of bone and mineral research : the official journal of the American Society for Bone and Mineral Research 18(4):705–715.
36. Chen W, Ma J, Zhu G, Jules J, Wu M, McConnell M, Tian F, Paulson C, Zhou X, Wang L, Li YP 2014 Cbfbeta deletion in mice recapitulates cleidocranial dysplasia and reveals multiple functions of Cbfbeta required for skeletal development. Proceedings of the National Academy of Sciences of the United States of America 111(23):8482–8487. [PubMed: 24850862]
37. Kuras L, Struhl K 1999 Binding of TBP to promoters in vivo is stimulated by activators and requires Pol II holoenzyme. Nature 399(6736):609–613. [PubMed: 10376605]
38. Zhang Y, Wang L, Song Y, Zhao X, Wong MS, Zhang W 2015 Renin inhibitor aliskiren exerts beneficial effect on trabecular bone by regulating skeletal renin-angiotensin system and kallikrein-kinin system in ovariectomized mice. Osteoporosis international : a journal established as result of cooperation between the European Foundation for Osteoporosis and the National Osteoporosis Foundation of the USA
39. Jules J, Chen W, Feng X, Li YP 2016 CCAAT/enhancer binding protein alpha (C/EBPalpha) is important for osteoclast differentiation and activity. The Journal of biological chemistry
40. Xie H, Ye M, Feng R, Graf T 2004 Stepwise reprogramming of B cells into macrophages. Cell 117(5):663–676. [PubMed: 15163413]

41. Jules J, Chen W, Feng X, Li YP 2016 CCAAT/Enhancer-binding Protein alpha (C/EBPalpha) Is Important for Osteoclast Differentiation and Activity. The Journal of biological chemistry 291(31): 16390–16403. [PubMed: 27129246]

42. Wang GL, Shi X, Haefliger S, Jin J, Major A, Iakova P, Finegold M, Timchenko NA 2010 Elimination of C/EBPalpha through the ubiquitin-proteasome system promotes the development of liver cancer in mice. J Clin Invest 120(7):2549–2562. [PubMed: 20516642]

43. Asagiri M, Takayanagi H 2007 The molecular understanding of osteoclast differentiation. Bone 40(2):251–264. [PubMed: 17098490]

44. Abram CL, Roberge GL, Hu Y, Lowell CA 2014 Comparative analysis of the efficiency and specificity of myeloid-Cre deleting strains using ROSA-EYFP reporter mice. Journal of immunological methods 408:89–100. [PubMed: 24857755]

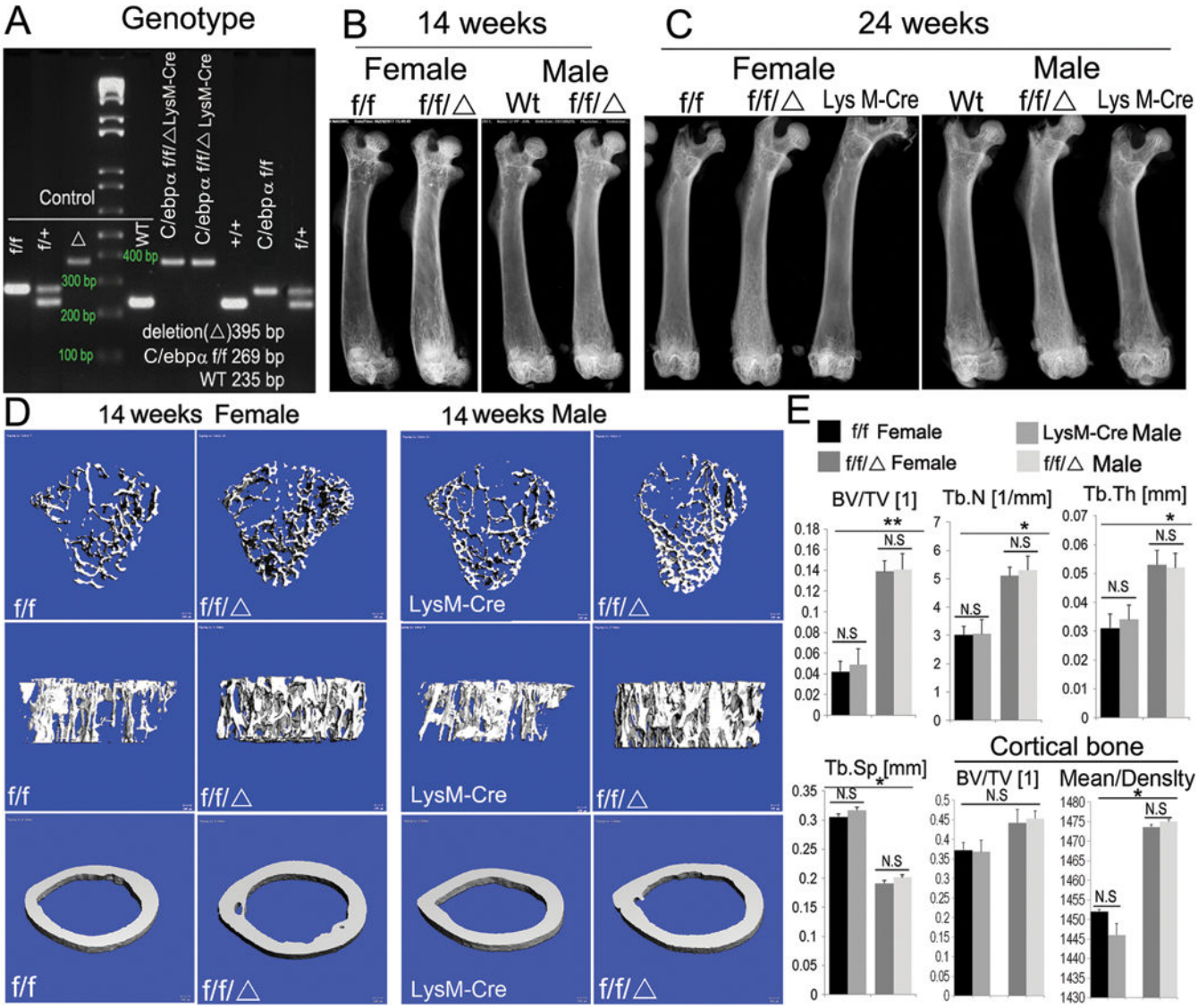

Figure 1. Mice with *LysM-Cre* mediated conditional knockout of *C/ebpα* developed osteopetrosis that becomes more severe as mice aged.

(**A**) Genotyping of C/ebpα$^{f/f}$ and C/ebpα$^{f/f}$LysM-Cre mice by PCR. Conditional knockout approach: excision through the endogenous promoter lysosome 2-Cre (LysM-Cre). Labels: (WT) wild-type; (f/+) heterozygote; (f/f/Δ) homozygous excision of C/ebpα; and (f/f) C/ebpα gene surrounded by loxp sites. (**B, C**) Radiographic analysis of male and female mouse femurs of 14-week-old (adult) and 24-week-old (aged) mice (n=60). (**D, E**) μCT and bone density analysis for both trabecular and cortical bones of 14-week-old male and female mouse femurs. Labels: (BV) bone volume, (TV) total bone volume, (Tb.N) trabecular number, (Tb.Sp) trabecular separation, (Tb.Th) trabecular thickness (n=8). C/ebpα$^{f/f}$ and LysM-Cre were used as control. Results are presented as mean ± SD. *p<0.05, **p<0.01. N.S, not significant.

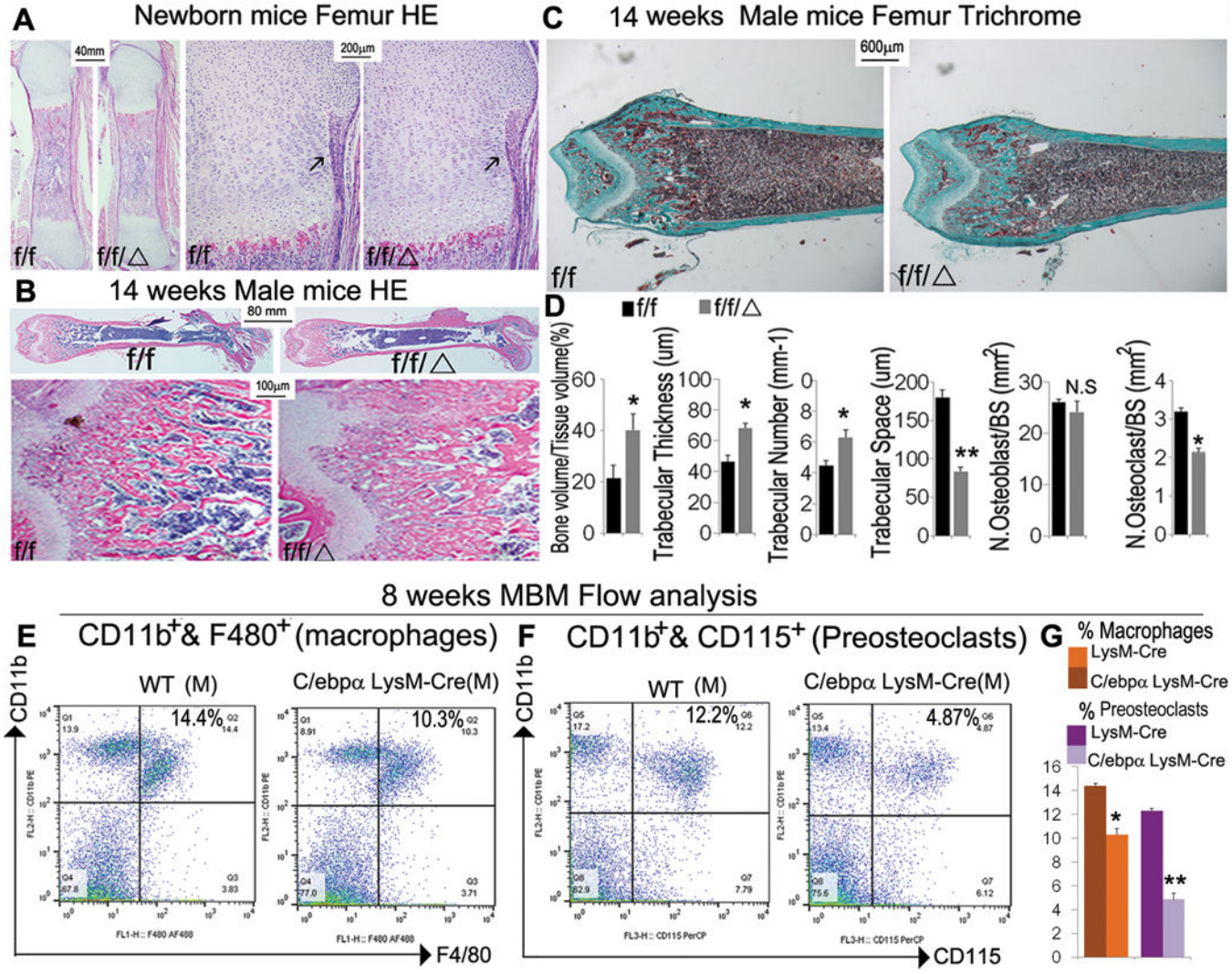

Figure 2. *C/ebpα*$^{f/f}$*LysM-Cre* mice showed significantly impaired OC function, with mild changes in macrophage development and a large reduction in preosteoclast number.

(A) Representative images of H&E staining of **(A)** newborn and **(B)** 14-week-old C/ebpα$^{f/f}$LysM-Cre (f/f/Δ) femurs with C/ebpα$^{f/f}$ (f/f) and LysM-cre as controls with high magnification of the epiphysis regions (n=10). (with 6 male and 6 female in each group). **(C)** Representative images of Goldner's Trichrome analysis and **(D)** quantification data for male 14-week-old C/ebpα$^{f/f}$LysM-Cre compared to C/ebpα$^{f/f}$ mouse femurs (n=16), which reconfirmed the severe osteopetrotic phenotypes in C/ebpα$^{f/f}$LysM-Cre while osteoblast and OC numbers of mutants and wild-type remained almost unchanged. Analyses were repeated for female mouse samples with similar findings. **(E, F)** Flow cytometry for **(E)** immune cell subtyping of CD11b+ F4/80+ macrophages and **(F)** CD11b+CD115+ OCs from 8-week-old mouse bone marrow. **(G)** Quantification of E and F. Results show means ± SD. of triplicate independent samples. *p<0.05, **p<0.01. N.S., not significant.

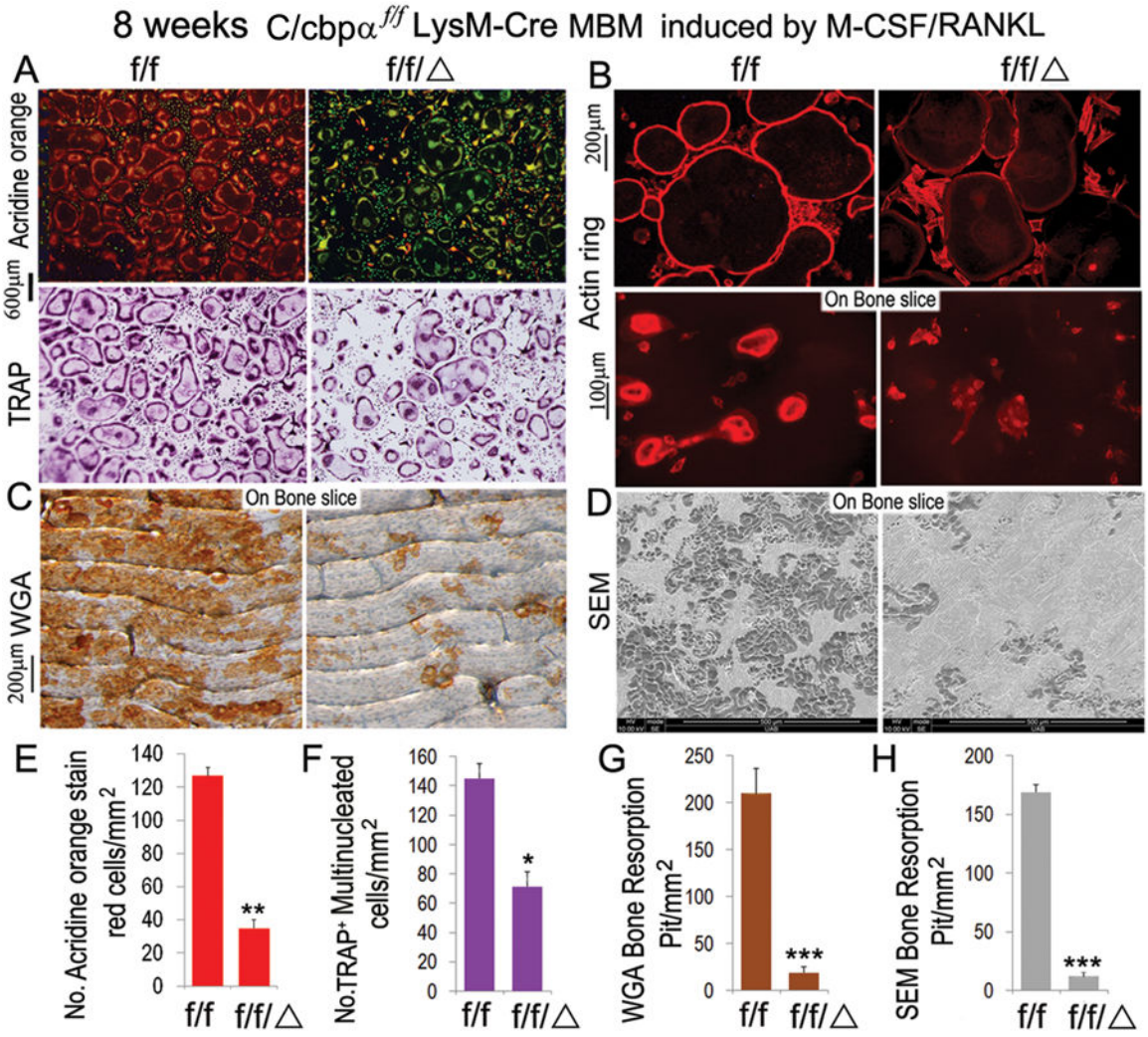

Figure 3. Conditional knockout of *C/ebpα* resulted in severely defective OC activation and function, leading to diminishing osteoclastic activity *in vitro*.

8-week-old C/ebpα$^{f/f}$LysM-Cre (f/f/Δ) and C/ebpα$^{f/f}$ (f/f) MBM were stimulated by M-CSF(10ng/mL)/RANKL(10ng/mL) to promote formation of multinucleated OCs. Assessment of OC differentiation and function was carried out at the end of day 5 post osteoclastogenic induction. (**A**) Acridine Orange staining and TRAP staining of C/ebpα$^{f/f}$LysM-Cre OCs with C/ebpα$^{f/f}$ OCs as control. Acidity (red-orange) and number of multinucleated OCs were significantly reduced in C/ebpα$^{f/f}$LysM-Cre OCs compared to C/ebpα$^{f/f}$ control. **(B)** F-actin ring formation assay on bone plates and bone slices shows disrupted or absent ringed structures of F-actin dots (actin rings) in M-CSF/RANKL-induced C/ebpα$^{f/f}$LysM-Cre OCs compared to C/ebpα$^{f/f}$ control. **(C)** Wheat germ agglutinin (WGA) staining to detect bone resorption pits. **(D)** Scanning electron microcopy (SEM) analysis of bone slices to detect bone resorption pits. **(E–H)** Quantification of A-D analyses. Number of positive cells were quantified per mm2 plate area NIH image software (ImageJ). Results are presented as mean ± SD, n=70. *p<0.05, **p<0.01, ***p<0.005.

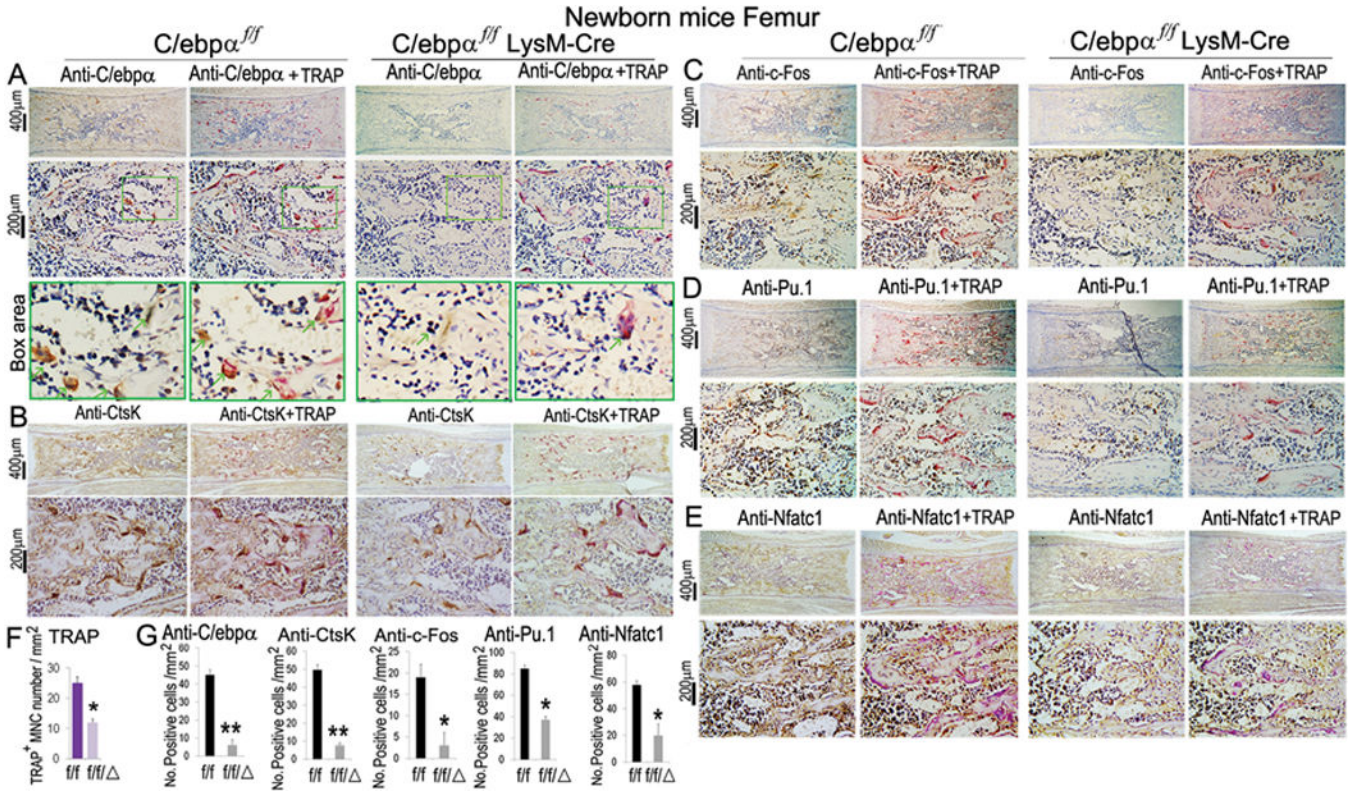

Figure 4. Conditional knockout of *C/ebpα* significantly reduced the expression of OC regulator genes (ie. *Nfatc1, c-fos*) and OC function genes (ie. *Ctsk, Atp6i*).

(A–D) Immunostaining using antibodies against **(A)** C/ebpα, **(B)** Ctsk, **(C)** c-Fos, **(D)** PU.1 and **(E)** Nfatc1 and their corresponding $TRAP^+$ co-stained images for newborn C/ebpα$^{f/f}$LysM-Cre (f/f/Δ) and C/ebpα$^{f/f}$ (f/f) mouse femurs. IHC analyses were also carried out using LysM-Cre mice showing similar results to C/ebpα$^{f/f}$ group. Lower panels in A-D show high magnification images of immunostaining results. **(F)** Quantification data for $TRAP^+$ cells. **(G)** Quantification data of staining results in A-E. Number of positive cells were quantified per mm2 plate area using NIH image software (ImageJ). Bars show means ± SD with n=30. *p<0.05, **p<0.01.

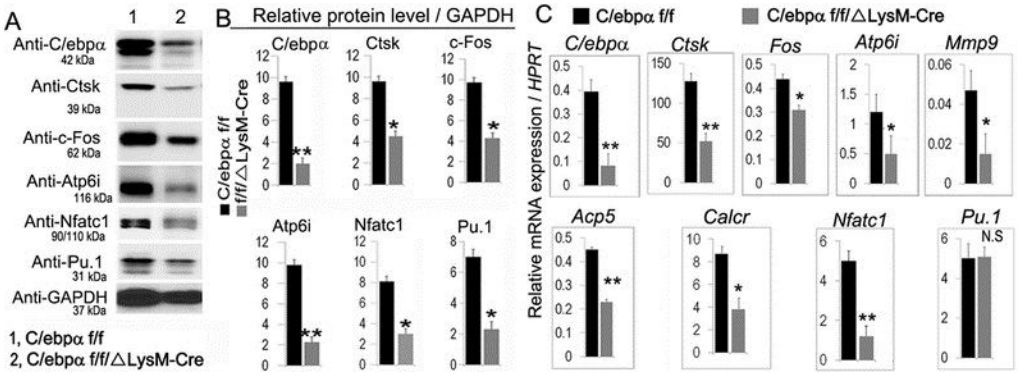

Figure 5: C/ebpα upregulated the expression of OC regulator genes and OC function genes at both protein and mRNA levels.

(A, B) Western blot and quantification data for C/ebpα$^{f/f}$LysM-Cre (f/f/Δ) and C/ebpα$^{f/f}$ (f/f) mice showing expressions of C/ebpα, Ctsk, C-Fos, Atp6i, Nfatc1, Pu.1 at the translational level. GAPDH is shown as loading control. **(C)** qRT-PCR of genes important for osteoclastogenesis and OC-specific function genes and a gene that is common to macrophages and OCs (i.*e.* Pu.1) in RANKL-induced MBM C/ebpα$^{f/f}$ and C/ebpα$^{f/f}$LysM-Cre mice. Hprt served as a loading control. Bars show means ± SD. (n=16). *p<0.05, **p<0.01. N.S, not significant.

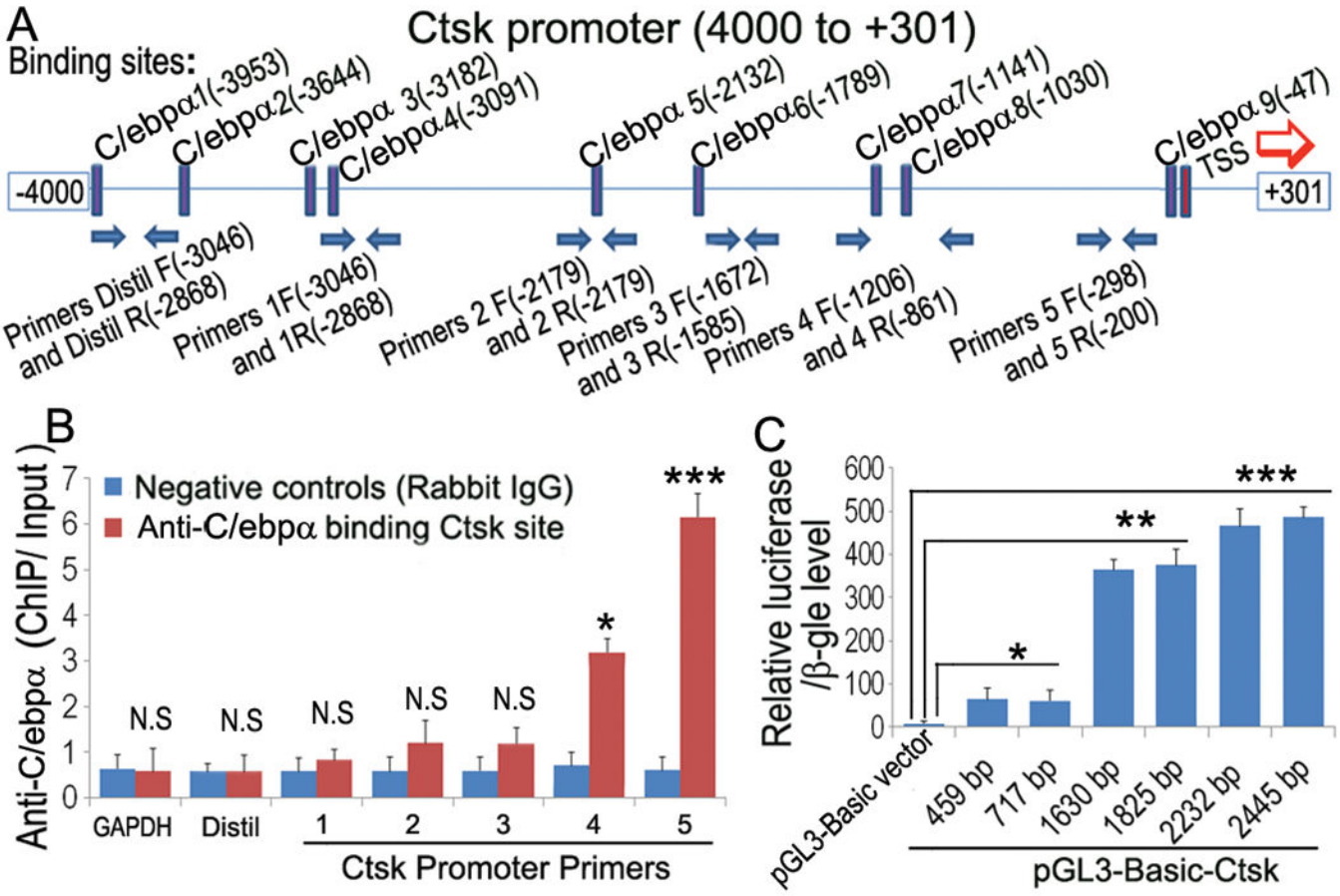

Figure 6: C/ebpα directly upregulates Ctsk expression through interactions with its promoter region.

(**A**) Schematic display of Ctsk (−4000/+301) promoter region: TSS (transcriptional start site), predicted C/ebpα-binding sites, and ChIP primers positions (F, Forward; R, Reverse). (**B**) ChIP analysis of C/ebpα binding to the Ctsk promoter in RANKL-induced mouse bone marrow (MBM) using primers as indicated on the x-axis. Results are presented as ChIP/ Input. **(C)** C/ebpα promoter fragments were inserted into pG13-basic vector. RAW 264.7 cells were transfected with pG13-C/ebpα−459bp,−717bp,−1630bp,−2232bp,−2445bp. Luciferase was detected at 48 hours post-transfection and normalized to β-gal activity. Results are presented as mean ± SD, n=10. *p<0.05, **p<0.01, ***p<0.005. N.S, not significant.

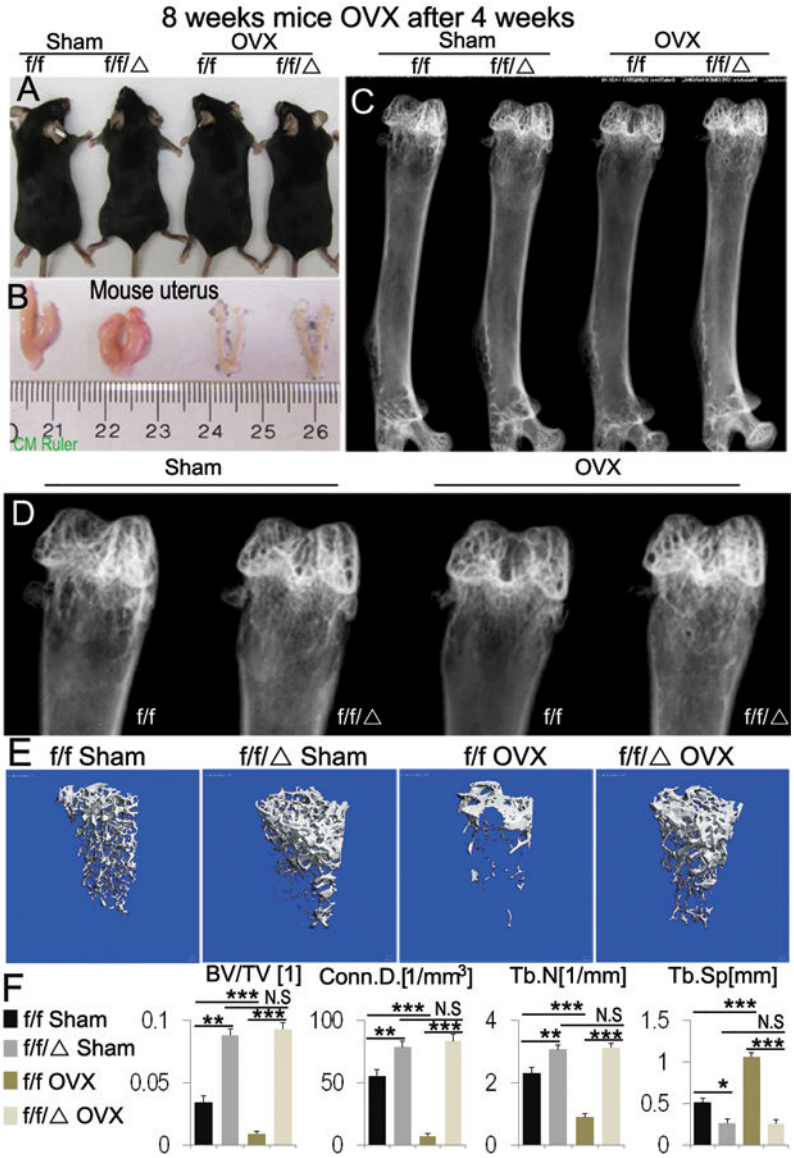

Figure 7. The deficiency of C/ebpα in OCs blocks ovariectomy (OVX)-induced bone loss in osteoporosis mouse model.

C/ebpα's roles in OVX-induced bone loss analysis were examined in 8-week-old C/ebpα$^{f/f}$ (f/f) and C/ebpα$^{f/f}$LysM-Cre (f/f/Δ) mice at 4 weeks after sham surgery and OVX (n=15). **(A)** Mouse photographic images and **(B)** assessment of uterine size to confirm the effects of OVX. **(C)** Representative images of radiographic analysis of mouse femurs. **(D)** High power image of the epiphysis regions from C data. No significant changes were found between sham- and OVX-C/ebpα$^{f/f}$LysM-Cre. Compared to OVX-C/ebpα$^{f/f}$ which displayed significant bone loss, C/ebpα-deficient mice retained normal bone mineral density similar to that of sham-C/ebpα$^{f/f}$ control. **(E)** μCT analysis of C/ebpα$^{f/f}$ and C/ebpα$^{f/f}$LysM-Cre mice femurs from C-D (n=4). **(F)** Quantification of E revealed that femurs from OVX-C/ebpα$^{F/F}$LysM-Cre mice retained significantly higher ratios of bone volume/tissue volume and increased trabecular numbers compared to OVX-C/ebpα$^{f/f}$ mice at 4 weeks post-operation. Labels: (BV) bone volume, (TV) total bone volume. (Conn.D) connectivity

density, (Tb.N) trabecular number, (Tb.Sp) trabecular separation, (Tb.Th) trabecular thickness. Bars show means ± SD. of triplicate independent samples. *p<0.05, **p<0.01, ***p<0.005. N.S, not significant.